THE PHOTOSPHERIC CONVECTION SPECTRUM

D. H. HATHAWAY[1], J. G. BECK[2], R. S. BOGART[2], K. T. BACHMANN[3],
G. KHATRI[3], J. M. PETITTO[3], S. HAN[4] and J. RAYMOND[4]

[1]*NASA/Marshall Space Flight Center, Huntsville, AL 35812, U.S.A.*
[2]*Stanford University, Stanford, CA, U.S.A.*
[3]*Birmingham-Southern College, Birmingham, AL 35254, U.S.A.*
[4]*Tennessee Technological University, Cookeville, TN 38505, U.S.A.*

Abstract. Spectra of the cellular photospheric flows are determined from observations acquired by the MDI instrument on the SOHO spacecraft. Spherical harmonic spectra are obtained from the full-disk observations. Fourier spectra are obtained from the high-resolution observations. The *p*-mode oscillation signal and instrumental artifacts are reduced by temporal filtering of the Doppler data. The resulting spectra give power (kinetic energy) per wave number for effective spherical harmonic degrees from 1 to over 3000. Significant power is found at all wavenumbers, including the small wavenumbers representative of giant cells. The time evolution of the spectral coefficients indicates that these small wavenumber components rotate at the solar rotation rate and thus represent a component of the photospheric cellular flows. The spectra show distinct peaks representing granules and supergranules but no distinct features at wavenumbers representative of mesogranules or giant cells. The observed cellular patterns and spectra are well represented by a model that includes two distinct modes – granules and supergranules.

1. Introduction

The Sun is the only star close enough to us to reveal details about its convective motions. These details challenge our models of stellar convection. We see at least two distinct cellular patterns – granules and supergranules. A third, mesogranules, was first reported by November *et al.* (1981) and a fourth, giant cells, has been reported recently (Beck, Duvall, and Scherrer, 1998). The mixing length theory for stellar convection works on the assumption that at any level within the convection there is one characteristic cell size, a size that is related to a pressure scale height at that level. The discrete cell sizes observed on the Sun suggest that stellar convection may be governed by something more than just the stratification of the layer. Simon and Weiss (1968) suggested that different cell sizes would be excited by the various ionization/recombination layers within the Sun. The current paradigm is that granules are driven by the recombination of hydrogen at 1 Mm depth, mesogranules by the second recombination of helium at 5 Mm depth, supergranules by the first recombination of helium at 15 Mm depth, and giant cells by the recombination of metals at the base of the convection zone (200 Mm depth). This paradigm has dominated our view of solar convection for decades.

Granules are most certainly convection cells. The observed characteristics (Bray, Loughhead, and Durrant, 1984) and numerical models (Stein and Nordlund, 1998) for granules both indicate that these features are driven by thermal convection in the highly superadiabatic layers just below the photosphere.

Supergranules were discovered in the Doppler velocity signal from the Sun by Hart (1954) but the flow was not initially associated with convection (Hart, 1956). Leighton, Noyes, and Simon (1962) made that connection somewhat later based on their observations of the surface-filling cellular structure of the flow.

Mesogranules were first extracted from Doppler velocity observations by November *et al.* (1981). The granules were unresolved in their observations and supergranules were removed by subtracting a spatially averaged signal. The remaining signal contained a cellular pattern with a characteristic size of about 5–10 Mm and lifetime of 2–3 hours. Wang (1989) questioned the existence of cells this size based on the lack of a peak in the power spectrum at these wavelengths from his analysis of similar Doppler data. He suggested that the original discovery was a result of the spatial filtering and might also be related to the presence of a residual p-mode signal. Chou *et al.* (1991) came to a similar conclusion from their analysis of a series of Doppler velocity images in which the p modes were filtered out. Ginet and Simon (1992) argued against this interpretation by modeling the data with both a supergranule and a mesogranule component. Chou *et al.* (1992) analyzed another set of observations that apparently did include a peak in the power spectrum at wavenumbers representative of mesogranules.

Giant cells have had a similarly controversial history. Their existence was suggested by Bumba and Howard (1965) based on the observed large-scale structure of the Sun's magnetic field. Simon and Weiss (1968) proposed that they should extend from the base of the convection zone to the surface as an efficient means of convective heat transport. Howard (1979) reported evidence for large-scale velocity features with amplitudes around 40 m s^{-1} in Doppler data from the Mount Wilson magnetograph. However, most attempts to observe giant cells in Doppler velocity observations have given upper limits for the velocity signal that are much less than this (Howard and LaBonte, 1980; LaBonte, Howard, and Gilman, 1981; Kuhn, 1983; Robillot *et al.*, 1984; Snodgrass and Howard, 1984). Durney *et al.* (1985) reported observing large-scale long-lived velocity patterns in the polar regions with amplitudes around 3 m s^{-1} and recently Beck, Duvall, and Scherrer (1998) reported observing long-lived cells with similar amplitudes in the form of narrow cells elongated in longitude.

Here we investigate the spectrum of cellular flows in the photosphere using the unprecedented data available from the Michelson Doppler Imager (MDI) (Scherrer *et al.*, 1995), on the ESA/NASA Solar and Heliospheric Observatory (SOHO). The data obtained with this instrument give continuous Doppler velocity observations with spatial resolution and coverage that includes features with sizes ranging from granules to the largest giant cells and with a temporal resolution that fully resolves the p-mode oscillations.

The full-disk data and the spectrum we obtain from them are described in the next section. A data simulation to confirm the nature of this spectrum is presented in the following section and our analysis of the high-resolution MDI data follows that. We find evidence for cellular features through the full range of the spectrum but with only two distinct spectral features – one representing granules and one representing supergranules.

2. The Data and Data Analysis

We analyzed Doppler velocity images acquired with the MDI instrument on SOHO. These 1024 by 1024 pixel images of the line-of-sight velocity are obtained from wavelength shifts in the Ni I 676.8 nm absorption line. Images are obtained at one minute intervals to resolve the p-mode oscillations. Although the data are designed for use in helioseismology, they are also appropriate for studies of the non-oscillatory photospheric flows. We chose full-disk data from May, June, and July of 1996 and high-resolution data from 30 July 1996 for this study. Solar activity was near its minimum during this time interval and the solar disk was often devoid of active regions for many days.

Sequences of images were averaged together with a weighted average, (Hathaway, 1988a), to remove the signal due to the p-mode oscillations. This particular temporal average is adapted from Libbrecht and Zirin (1986). It uses 31 images and reduces the p-mode signal amplitude at 2–4 mHz by a factor of about 500. The relative weights are given by

$$w(\Delta t) = \exp[\Delta t^2/(2a^2)] - \exp[b^2/(2a^2)][1 + (b^2 - \Delta t^2)/(2a^2)] , \qquad (1)$$

where Δt is the time difference from the central image, $b = 16$ is the half length of the filter and $a = 8$ is the full width at half maximum all measured in minutes. This temporal filter is largely Gaussian in shape so its frequency response is also largely Gaussian. The filter is truncated at $\Delta t = \pm b$ where both the filter weight and its first derivative vanish. The full frequency response of this filter is shown in Figure 1 along with the response of a similar 17-min filter ($b = 9$ and $a = 4$) and a simple 60-min average.

The 31-min filter reduces the p-mode signal to a level of about 1 m s^{-1}. One disadvantage of this filter is its length. Although more than 50% of the weight is on the central 9 minutes, solar rotation still introduces substantial smearing of these relatively high resolution images. This problem is reduced through a 'derotation' of the images by sampling each image in the series at positions that are translated using the spectroscopic rotation profile of Snodgrass and Ulrich (1990).

The filtered data stream is sampled at 15 minute intervals over 62 days from 24 May 1996 to 24 July 1996. These full-disk data are processed using the spherical harmonic decomposition method described in Hathaway (1987) and Hathaway (1992) to determine and remove the velocity signals due to the axisymmetric flows
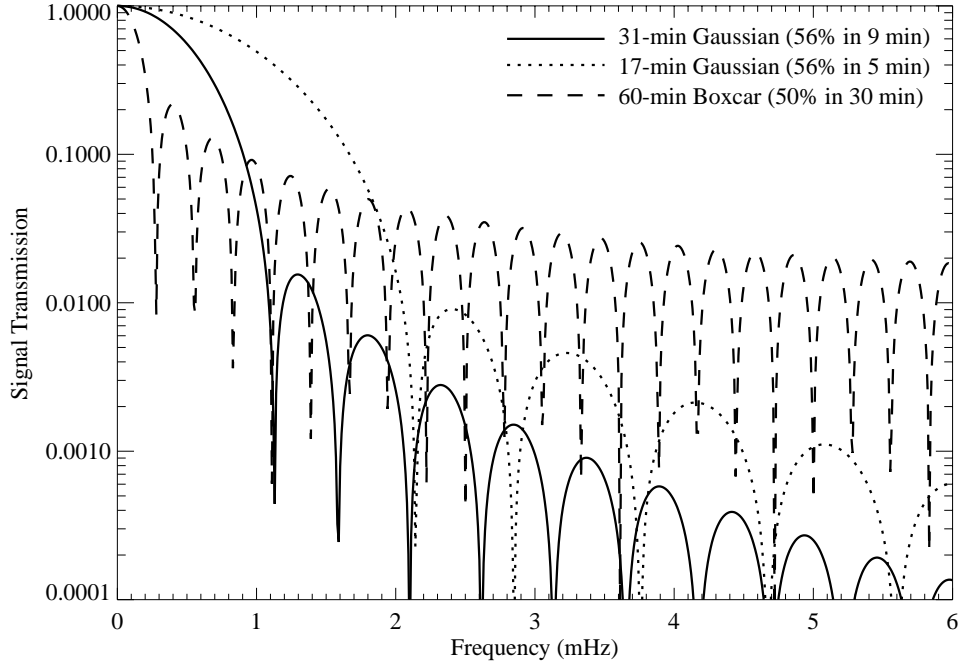
Figure 1. Response (signal transmission) of *p*-mode filters as functions of frequency. The *p* modes have most of their power in the 2–4 mHz frequency band. Several percent of the signal in this band is transmitted by the 60-minute filter. Less than 1% is transmitted by the 17-min weighted filter and less than 0.3% is transmitted by the 31-min filter.

(rotation, differential rotation, and meridional flow) and the unresolved granulation (the convective blue-shift signal). The remaining signal is dominated by the cellular convective flows. An example of this signal is shown in Figure 2. Typical velocities are 300 to 400 m s^{-1} and are dominated by the supergranule flows.

This Doppler velocity signal, *V*, is mapped onto heliographic coordinates (co-latitude θ and longitude ϕ) and then projected onto spherical harmonics (Y_ℓ^m) such that

$$V(\theta, \phi) = \sum_\ell \sum_{m=-\ell}^{\ell} A_\ell^m Y_\ell^m(\theta, \phi) , \tag{2}$$

where the A_ℓ^m are complex amplitudes. The spherical harmonic degree, ℓ, gives the characteristic size of a component of the flow with wavelength, λ, given by

$$\lambda = \frac{2\pi R_\odot}{\ell} \approx \frac{4400}{\ell} \text{ Mm} . \tag{3}$$

The spherical harmonic order, *m*, gives the wavenumber in longitude and determines the shape of the cells for that particular spherical harmonic component.

The spectra for the convective flow components are given by the complex amplitudes for the spherical harmonic components in each image. These spectra are
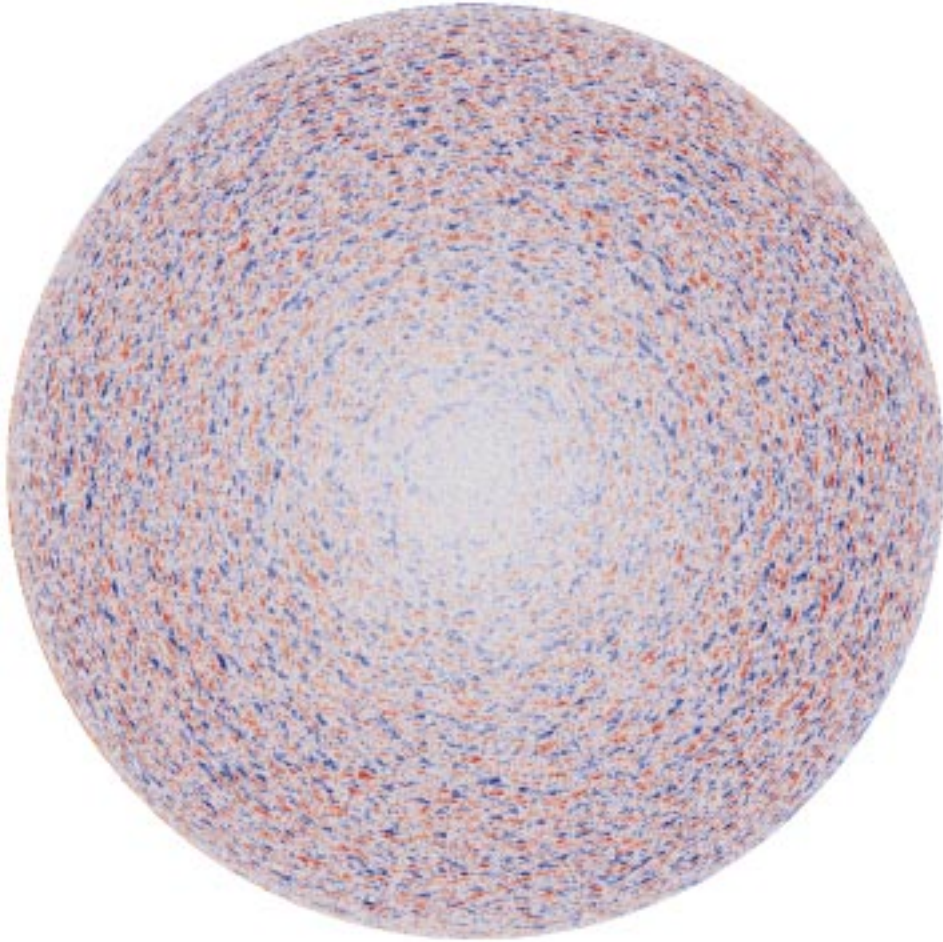
Figure 2. The cellular flows in the full-disk MDI data from 01:00 UT on 24 May 1996. Red-shifted flows are red, blue-shifted flows are blue. The flow field is dominated by the largely horizontal flows in the supergranules with typical velocities of 300 to 400 m s^{-1}.

filtered further by removing the stationary component from the data stream. This stationary component (the temporal average of the complex spectra) results from an incomplete removal of the axisymmetric flows as well as from instrumental artifacts. The power at a given wavenumber, ℓ, is given by

$$P(\ell) = \sum_{m=-\ell}^{\ell} |A_\ell^m|^2 \;. \tag{4}$$

The average power spectrum for the convective flows is shown in Figure 3. This spectrum rises to a prominent peak at $\ell \sim 120$ representing supergranules with wavelengths of about 35 Mm. The power decreases monotonically out to the
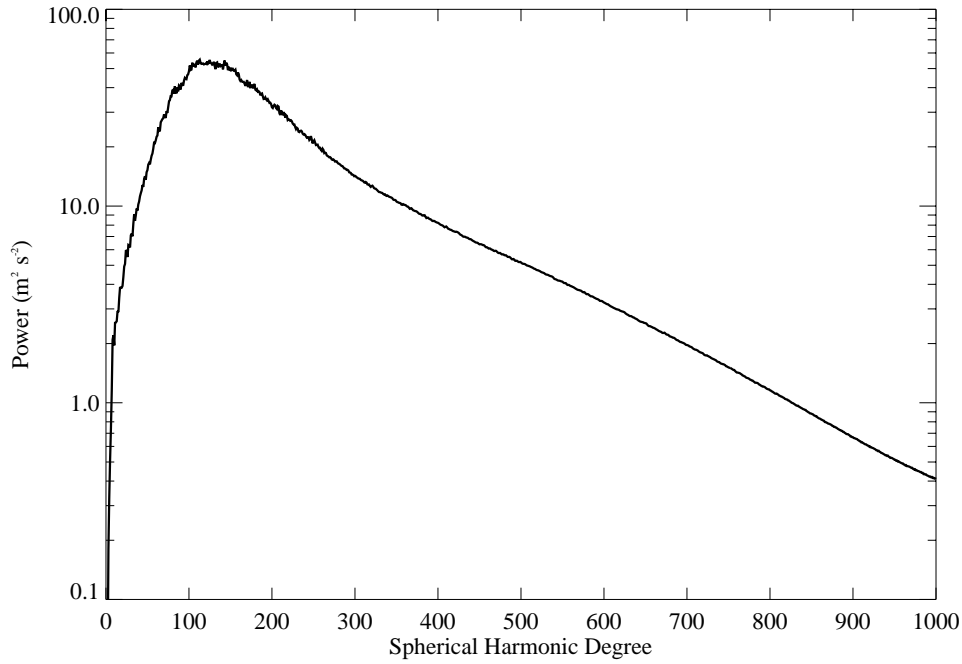
Figure 3. The average observed power spectrum for the cellular photospheric flows in the full-disk MDI data. The peak at $\ell \sim 120$ represents supergranules. There are no significant features to indicate that either mesogranules ($\ell \sim 600$) or giant cells ($\ell < 30$) are distinctly different from supergranules.

very highest wavenumbers we resolve with these data. We find no obvious features in the spectrum that would suggest distinct modes of convection at the size of mesogranules ($\ell \sim 600$) or giant cells ($\ell < 30$).

This does not deny the existence of cells at these wavenumbers. Both the spectrum (Figure 3) and the data visualization (Figure 2) indicate the presence of cells with sizes characteristic of mesogranules. There is also good evidence within these data for the existence of cells with sizes characteristic of giant cells. We find power at those wavenumbers ($\ell < 30$) although the power is greatly reduced from the peak of the spectrum at $\ell \sim 120$ and rapidly diminishes toward smaller wavenumbers. Movies constructed from the signal at these small wavenumbers show that these cells persist for a 14-day disk passage and rotate with the solar rotation rate. Taking the Fourier transform of the time string of spectral coefficients, $A_\ell^m(t)$ and summing over ℓ for each longitudinal wavenumber m, we find a distinct ridge of power representing the rotation of these cells. This characteristic ridge is shown in Figure 4.
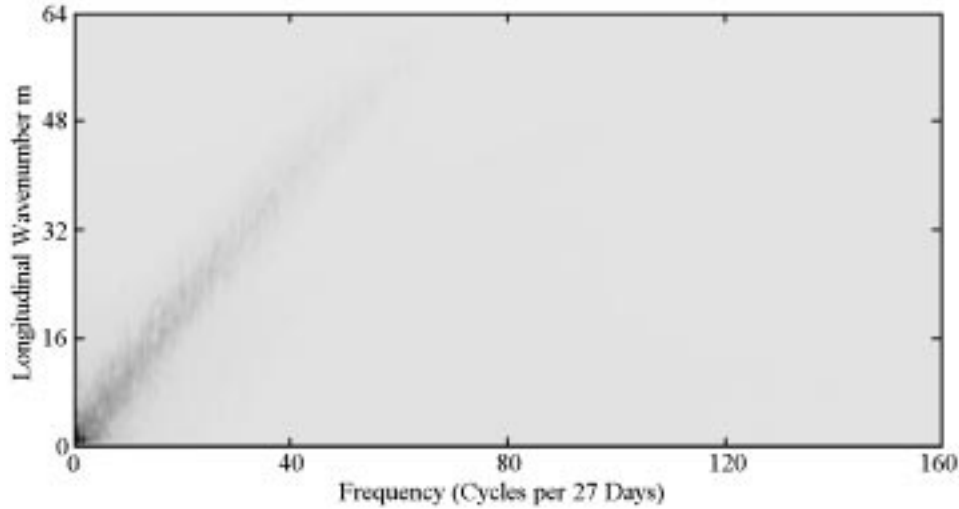
Figure 4. The power as a function of longitudinal wavenumber *m* and temporal frequency for the largest cells ($\ell < 64$). The ridge in power at frequencies of *m* cycles per rotation period (27 days) indicates the presence of a small-wavenumber pattern that rotates at about the solar rotation rate.

3. Data Simulation

Further support for the identification of the spectral features is obtained from data simulations. Doppler velocity images at 1-min intervals are constructed from an input spectrum using the method described by Hathaway (1988b).

The input spectrum requires three complex amplitudes for each spherical harmonic component in order to produce a vector velocity field on a spherical surface. The three amplitudes represent the amplitude of the radial flow, the amplitude of the poloidal flow (divergent horizontal flows), and the amplitude of the toroidal flow (vortical horizontal flows). For these simulations we only include the poloidal flows. The radial flows are much weaker than the horizontal flows as evidenced by the lack of signal at disk center in Figure 2. The toroidal flows are also much weaker than the poloidal flows as evidenced by the lack of any systematic tilt in the zero velocity lines in Figure 2. (For poloidal flows the zero line-of-sight velocity lines through the centers of cells are parallel to the limb. For toroidal flows these lines are perpendicular to the limb.)

The vector velocity field produced from this input spectrum is projected onto the line-of-sight to produce a Doppler image. The Doppler images are processed through the same temporal filtering and derotation procedures as are used on the full-disk MDI data and similar convection spectra are produced. The resulting spectra are compared to those from the MDI data and the input spectrum is adjusted until a good match is obtained.

The resulting spectrum for the simulated data is shown in Figure 5. The match between the spectra shown in Figures 3 and 5 is excellent. The only deviations are
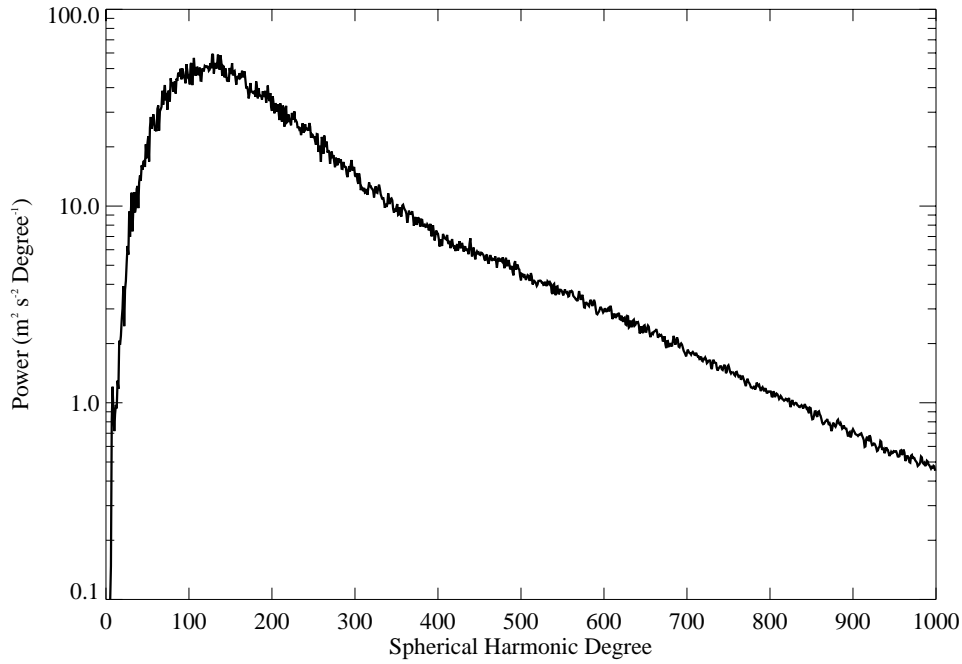
Figure 5. The observed power spectrum for the data simulation. The general shape of this spectrum matches that of the MDI data shown in Figure 3.

in the details due to the use of a single sample for the simulated data instead of the hundreds of samples incorporated in the MDI spectrum.

Matching spectra do not necessarily imply matching data. While no attempt has been made to produce a point-by-point match in the resulting velocity patterns, we would hope to produce data that have the same visual appearance as the real data. A comparison of the Doppler velocity patterns from MDI and from the simulation is shown in Figure 6. It is virtually impossible to distinguish between the real and the simulated data except in minor details.

The simulated data are a good representation of the real data as seen in both the spectra and the data visualization. An advantage of the simulated data is that we have the actual vector velocities at every point on the surface. This allows us to calculate the kinetic energy associated with each spherical harmonic component without the problems associated with line-of-sight projections and foreshortening. The input kinetic energy spectrum for the simulated data is shown in Figure 7. It is represented by just two components: one for the supergranules with a peak at $\ell \sim 120$ and the second for the granules with a peak beyond the end of the full-disk spectrum limit.

Convection Pattern 1996 May 24
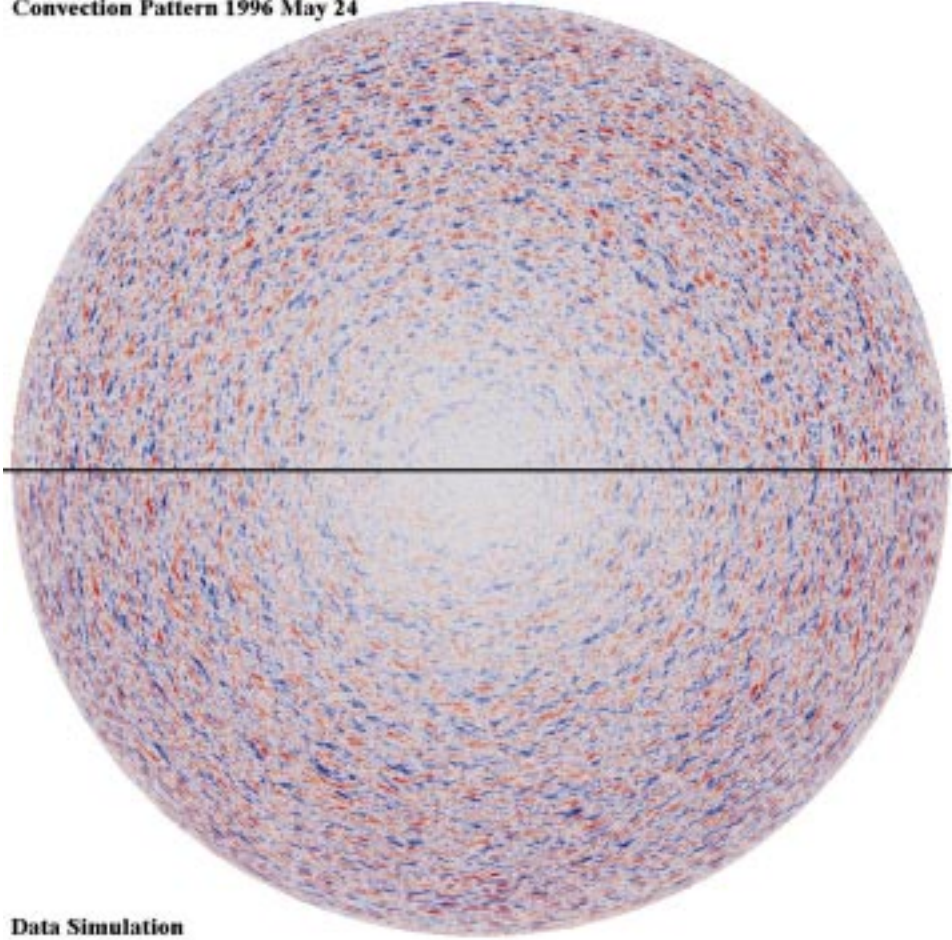
Data Simulation

Figure 6. A comparison of the cellular flows from MDI (*top*) and the data simulation (*bottom*).

4. High-Resolution Data Analysis

The MDI instrument also has a high-resolution mode in which the solar image is magnified by an additional factor of three. Granules are better resolved at this magnification but the field of view includes only a portion of the solar disk. Data obtained in this mode on 30 July 1996 were acquired and processed in a similar manner. The images are averaged together using the 31-min temporal filter and derotated images. The axisymmetric flows (rotation, differential rotation, and meridional flow), along with the remaining component of the convective blue shift, are effectively removed by subtracting a second-order polynomial surface fit.

The resulting data are shown in the bottom panel of Figure 8 together with a corresponding segment of the full-disk data in the top panel. The Doppler signal associated with granules is evident in the smallest features in this image. Since the
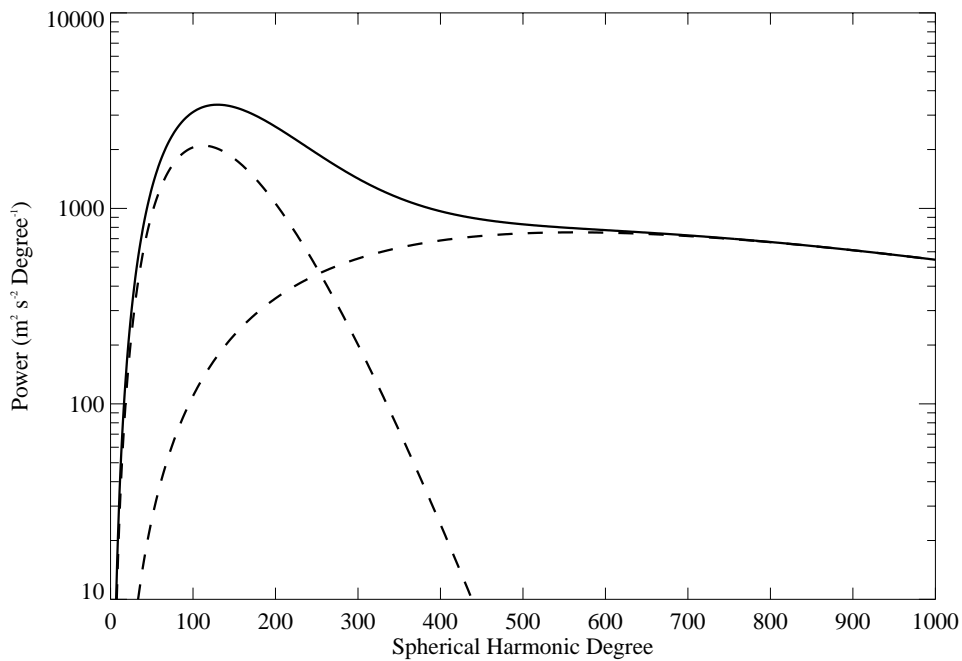
Figure 7. The kinetic energy spectrum used as input to the data simulation. Only two spectral components are required: a supergranule component with a peak at spherical harmonic degree $\ell \sim 120$ and a granule component with a peak beyond $\ell = 1000$.

fluid flow within the granulation has a substantial radial component, this flow component is readily seen in the blue-shifted grains seen at disk center. Supergranules are also readily visible at points away from disk center. Cells of intermediate size can also be seen and are particularly evident in the lower resolution full-disk data.

The high-resolution data, with the p modes and axisymmetric flows removed, are analyzed to determine the power spectrum of the higher wavenumber flow components. The data array is apodized with a Hanning (cosine) weighting function to reduce the spectral artifacts associated with the edges of the array. The resulting data are processed with a 2D FFT and the spectral power is summed on annuli about the wavenumber origin. The velocity spectrum for this single high-resolution dataset is shown in Figure 9. The supergranule peak at $\ell \sim 120$ still dominates but the granule peak is now more evident. In these high-resolution data the power rises from a local minimum at $\ell \sim 400$ to a broad plateau at $\ell \sim 1000$ before falling at higher wave numbers. This drop in power beyond $\ell \sim 1000$ is almost certainly artificial. The granules are not fully resolved with these data and their lifetimes are similar in length to the length of the temporal filter. Both of these characteristics should diminish the power observed at high wavenumbers. In addition, since the individual granules are advected by the larger scale flows a simple derotation of the images does not keep the granules observed in the images fully aligned.
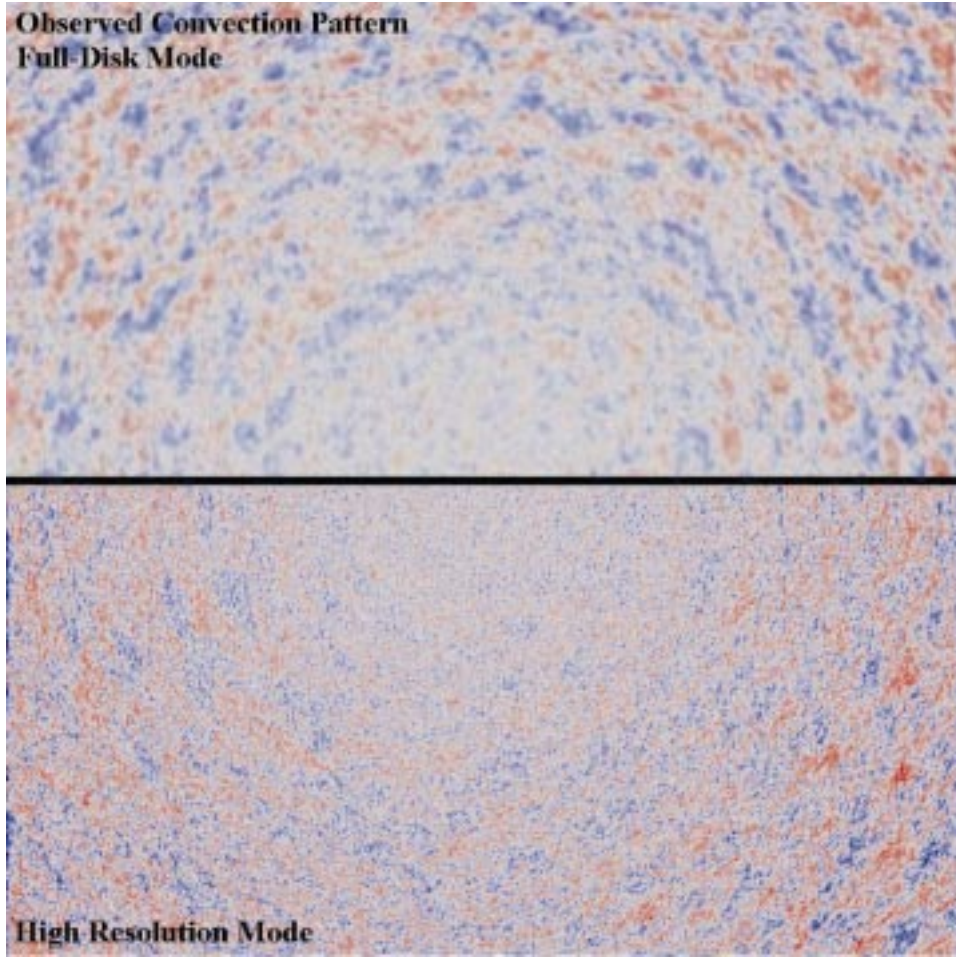
Figure 8. High-resolution data (*bottom*) compared with the low-resolution full-disk data (*top*). The granules are better resolved in the high-resolution data but supergranules are also readily apparent.

5. Discussion

The results of this study show that a broad spectrum of cellular flows exist in the photosphere. Distinct features in the spectrum are seen for the granules and the supergranules. Cells with sizes corresponding to mesogranules and giant cells also exist but there is no evidence to suggest that they are represented by modes of convection distinctly different from supergranules. There is, in fact, a distinct dip in the spectral power at the wavenumbers where mesogranules should begin to dominate. The two distinct spectral components (granules and supergranules) are evident in both the full-disk data and the high-resolution data. Studies of the 'background' solar velocity spectrum for p modes also show that the 'mesogranule' component must be small compared to supergranules and granules (Pallé *et al.,* 1995).
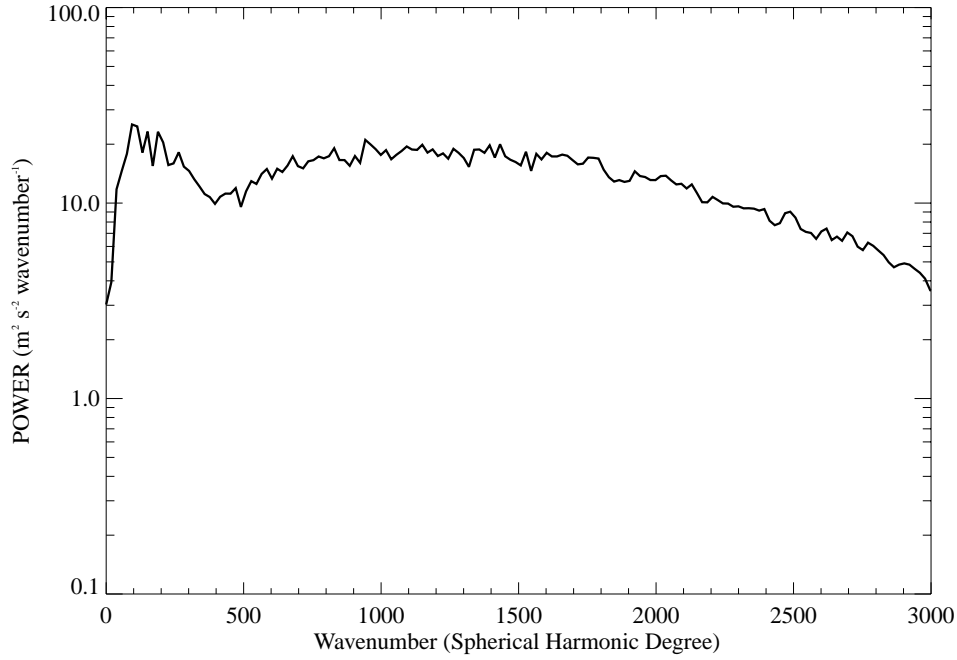
Figure 9. Doppler velocity power spectrum for the high-resolution MDI data. The supergranule peak at $\ell \sim 120$ is prominent as is the broad peak at $\ell > 1000$ representing granules. There are no spectral features suggesting distinct components for mesogranules or giant cells.

Artificial data were constructed to mimic the full-disk data. The simulated data match the real data in both spectral content and visual appearance and only require two components for their construction: a supergranule component with peak power at $\ell \sim 120$ and a granule component with peak power beyond $\ell = 1000$. Additional improvements could be made to the artificial data. We have neglected both radial flows and toroidal flows (horizontal flows with vorticity but without divergence). The neglect of the radial flows should be a good approximation for the wavenumbers representative of supergranules but becomes increasingly unrealistic at the higher wavenumbers representative of granules. Solar rotation should not induce systematic toroidal flows for the larger wavenumbers but might be important for the smallest wavenumbers that are representative of the largest supergranules. However, adding these improvements to the simulated data should not alter our conclusions concerning mesogranules and giant cells.

We conclude that mesogranules do not exist as a distinct mode of convection in the solar photosphere. Cellular structures corresponding to the reported sizes of mesogranules can indeed be found but they do not represent anything other than large granules or small supergranules. Previous studies of mesogranules are based on techniques that filter out cells with sizes traditionally associated with granules and supergranules and then focus on the characteristics of the remaining signal.

There is no evidence here that these cells are distinctly different from granules or supergranules. Any distinct mode of convection related to mesogranules would have to have a velocity amplitude at least an order of magnitude smaller that that due to supergranules and granules with similar sizes.

Likewise, we conclude that giant cells do not exist as a distinct mode of convection in the solar photosphere. Large, giant-cell-sized structures can be found but they correspond to the large wavelength end of the supergranule phenomenon. There is nothing in the spectrum to indicate that the observed cells are anything other than large supergranules. Any distinct mode of convection related to giant cells would also have to have a velocity amplitude at least an order of magnitude smaller than that due to supergranules of similar sizes.

The lack of any evidence for mesogranules or giant cells that are distinctly different from supergranules suggests a possible re-evaluation of our concepts concerning convection in the solar photosphere. The convective nature of granulation is well established by both observation and theory. If neither mesogranules nor giant cells are represented in the photospheric flows then what do supergranules represent? Good evidence for the convective nature of supergranules is lacking. The radial flows associated with supergranules are weak and there is not an associated intensity or temperature pattern. November (1994) has suggested that supergranule flows are shallow and helioseismic measurements (Duvall *et al.*, 1997) tend to support that suggestion. The very rapid rotation rate of the supergranule pattern (Snodgrass and Ulrich, 1990) also raises questions concerning the nature of supergranulation. Precisely how these flows are driven and what determines their characteristic size are once again unanswered questions.

Acknowledgements

References

Beck, J. G., Duvall Jr., T. L., and Scherrer, P. H.: 1998, *Nature* **394**, 653.
Bray, R. J., Loughhead, R. E., and Durrant, C. J.: 1984, *The Solar Granulation,* Cambridge University Press, Cambridge.
Bumba, V. and Howard, R.: 1965, *Astrophys. J.* **141**, 1502.

Chou, D.-Y., LaBonte, B. J., Braun, D. C., and Duvall Jr., T. L.: 1991, *Astrophys. J.* **372**, 314.

Chou, D.-Y., Chen, C.-S., Ou, K.-T., and Wang, C.-C.: 1992, *Astrophys. J.* **396**, 333.

Durney, B. R., Cram, L. E., Guenther, D. B., Keil, S. L., and Lytle, D. M.: 1985, *Astrophys. J.* **292**, 752.

Duvall, Jr., T. L., Kosovichev, A. G., Scherrer, P. H., Bogart, R. S., Bush, R. I., De Forest, C., Hoeksema, J. T., Schou, J., Saba, J. L. R, Tarbell. T. D., Title, A. M., Wolfson, C. J., and Milford, P. N.: 1997, *Solar Phys.* **170**, 63.

Ginet, G. P. and Simon, G. W.: 1992, *Astrophys. J.* **386**, 359.

Hart, A. B.: 1954, *Monthly Notices Royal Astron. Soc.* **114**, 17.

Hart, A. B.: 1956, *Monthly Notices Royal Astron. Soc.* **116**, 38.

Hathaway, D. H.: 1987, *Solar Phys.* **108**, 1.

Hathaway, D. H.: 1988a, *Solar Phys.* **117**, 1.

Hathaway, D. H.: 1988b, *Solar Phys.* **117**, 329.

Hathaway, D. H.: 1992, *Solar Phys.* **137**, 15.

Howard, R.: 1979, *Astrophys. J.* **228**, L45.

Howard, R. and LaBonte, B. J.: 1980, *Astrophys. J.* **239**, 738.

Kuhn, J. R.: 1983, *Astrophys. J.* **264**, 689.

LaBonte, B. J., Howard, R., and Gilman, P. A.: 1981, *Astrophys. J.* **250**, 796.

Leighton, R. B., Noyes, R. W., and Simon, G. W.: 1962, *Astrophys. J.* **135**, 474.

Libbrecht, K. and Zirin, H.: 1986, *Astrophys. J.* **308**, 413.

November, L. J.: 1994, *Solar Phys.* **154**, 1.

November, L. J., Toomre, J., Gebbie, K. B., and Simon, G. W.: 1981, *Astrophys. J.* **245**, L123.

Pallé, P. L., Jiménez, A., Pérez Hernández, F., Régulo, C., Roca Cortés, T., and Sánchez, L.: 1995, *Astrophys. J.* **441**, 952.

Robillot, J. M., Bocchia, R., Fossat, E., and Grec, G.: 1984, *Astron. Astrophys.* **137**, 43.

Simon, G. W. and Weiss, N. O.: 1968, *Z. Astrophys.* **69**, 435.

Scherrer, P. H., Bogart, R. S., Bush, R. I., Hoeksema, J. T., Kosovichev, A. G., Schou, J., Rosenberg, W., Springer, L., Tarbell, T. D., Title, A., Wolfson, C. J., Zayer, I. and the MDI Engineering Team: 1995, *Solar Phys.* **162**, 129.

Snodgrass, H. B. and Howard, R.: 1984, *Astrophys. J.* **284**, 848.

Snodgrass, H. B. and Ulrich, R. K.: 1990, *Astrophys. J.* **351**, 309.

Stein, R. F. and Nordlund, Å.: 1998, *Astrophys. J.* **499**, 914.

Wang, H.: 1989, *Solar Phys.* **123**, 21.